Adaptive Suppression of Biodynamic Interference in Helmet-Mounted Displays and Head Teleoperation

S. Lifshitz* and S. J. Merhav†
Technion—Israel Institute of Technology, Haifa, 32000 Israel

This paper addresses errors caused by vibration or turbulence in airborne helmet displays and teleoperation. It is shown by analysis and computer simulations that a modified version of the least-mean-squares adaptive noise suppression algorithm facilitates the separation of the large voluntary head movements from the vibration-induced small nonvoluntary head motion. Thus, the effects of the biodynamic interference can be essentially removed. The results also indicate that errors in head-tracking teleoperated devices can essentially be suppressed. Extensive man-in-the-loop laboratory simulations that validate the method are described.

I. Introduction

SYSTEM teleoperation by pilot head motion and presentation of computer-generated symbols and flight information in helmet-mounted displays is emerging as a promising technology in modern avionic systems. Head teleoperation is potentially an effective method for instinctive and rapid aiming of radar antennas, missile seeker heads, or laser designators. In addition, it relieves the hands of the pilot for other vital manual tasks in increasingly complex airborne environments. Helmet-mounted displays (HMD) can, in principle, be the ultimate solution in merging computer-generated displays with the outside scene, thus embracing the entire field of view available to the pilot. Therefore, the HMD potentially relieves the pilot from the troublesome need to share his attention between the all-aspect outside scene and a restrictive cockpit-mounted panel or head-up display.

However, a potential shortcoming of head teleoperation and HMDs is their vulnerability to biodynamic interference resulting from vibration, atmospheric turbulence, or self-induced vehicle motion. These interferences can cause substantial random aiming errors and apparent display blurring that may seriously impair pilot performance. Two kinds of biodynamic interference exist, namely, 1) additive interferences due to nonvoluntary limb motions caused by, and correlated with, vibration,[1,2] and 2) nonadditive interferences resulting from the disturbances in the central nervous system caused by the body and head vibrations, uncorrelated with them, but monotonically increasing with their intensity.[3,4] Head vibration causes relative angular motion of the HMD with respect to the line of sight of the eye, which is inertially stabilized by the vestibular system. Consequently, as a result of the apparent display shift, image blurring occurs, resulting in substantial degradation of reading speed and probability of correct character recognition.[5,6] This neuromotor stabilization, known as the vestibulo-ocular reflex (VOR), is effective in the frequency range of 2–10 Hz.[7] Wells and Griffin[6,8] conducted experiments to cancel this blurring by shifting the display in the opposite direction with an amplitude equal to the measured head motion which was determined by an approximate double integration of head angular acceleration. They succeeded in demonstrating the effectiveness of the concept, but the imperfection of the integration caused substantial transients in the display position in the presence of large angular head motion.

Received Jan. 24, 1990; revision received Oct. 2, 1990; accepted for publication Oct. 2, 1990.

*Graduate Student, Department of Aerospace Engineering.
†Professor, Head Flight Control Laboratory, Department of Aerospace Engineering.

In this paper, a method for display stabilization, based on a modified adaptive noise cancellation (ANC), is described.[9] It is designed to fulfill the following requirements: 1) suppression of the additive nonvoluntary head motion due to vibration even in the presence of large voluntary head motion, and 2) rapid adaptation to changing parameters in the biodynamic model of the pilot due to changes in posture and muscle tone.

Extensive computer simulations with a linear biodynamic model were performed. These demonstrated the effectiveness of the adaptive filter (AF) in suppressing the effects of additive biodynamic interference. Subsequently, extensive man-in-the-loop experiments were conducted on a six-degree-of-freedom simulator that was driven by vertical vibration commands representing typical helicopter vibration spectra. The results of these tests proved to have excellent correspondence with the computer simulations and they demonstrated their effectiveness under essentially realistic flight conditions.

II. Stabilization of Helmet Displays

The principle of operation of helmet display stabilization is described with the aid of Fig. 1. The aircraft A/C is viewed through the transparent helmet visor. The hexagon S represents a reticle symbol element generated in the helmet-mounted cathode ray tube (CRT) and is projected to optical infinity. Platform accelerations a excite the biodynamic angular head motion α which is detected by the six-degree-of-freedom head motion sensor P, providing the voluntary head motion signal U_c along with the signal U_b, which represents the additive nonvoluntary head motion. The biodynamic angular head motion α causes S to move with respect to the line of sight to A/C, which remains fixed on the retina because of the vestibulo-ocular reflex. The search and track voluntary head motion, also detected by P, is denoted by U_c. The total head motion signal, $U_t = U_c + U_b$, would normally drive the teleoperated device inducing aiming errors due to U_b. The block Y_b, shown by dotted lines, represents the biodynamic model which can be representative of different limbs or body elements. The relative angular deviation α between the stabilized line of sight and the reticle S can cause apparent display blurring indicated by S'. The display stabilization signals are provided by the adaptive filter as follows. Platform-mounted inertial sensors, consisting of accelerometers or gyroscopes, sense the signal a' that is linearly correlated with a and the angular head motion α. The output $\hat{U}_b$ of AF is compared to $U_t = U_c + U_b$. The error e drives the adaptive algorithm in AF so that its internal parameters automatically adjust to minimize e^2. It is easily seen that this occurs when $U_b - \hat{U}_b \triangleq \tilde{U}_b \to 0$. This method, known as adaptive noise canceling (ANC),[9] considerably reduces the biodynamic interference component U_b without essentially affecting U_c. In order to stabilize computer-generated symbols such as S, $\hat{U}_b$ is fed into

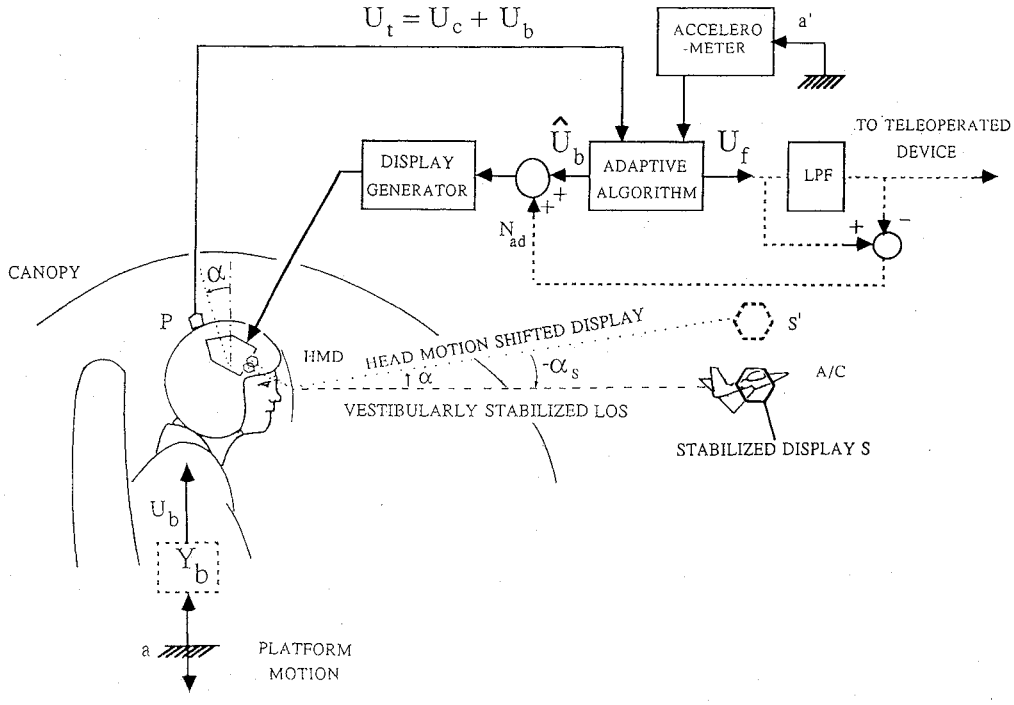

Fig. 1 HMD stabilization: principle of operation.

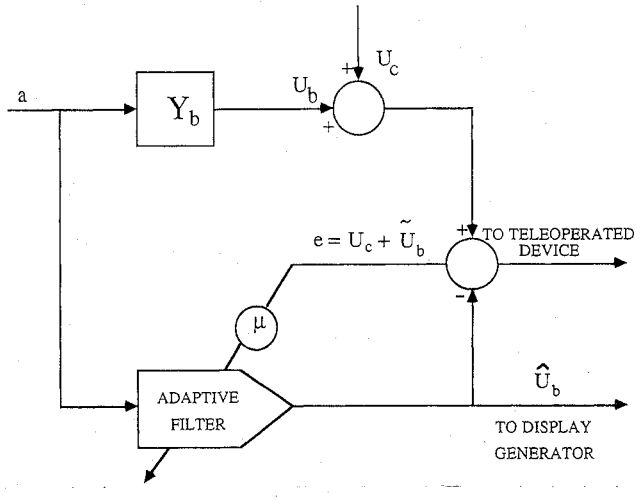

Fig. 2 Basic LMS algorithm for suppression of biodynamic interference in HMD and head teleoperation.

the display generator, so that S is shifted by $\alpha_s = -\alpha$, which is thus stabilized with respect to the line of sight and consequently display blurring is essentially suppressed. The estimated voluntary head motion $U_f \triangleq U_t - \hat{U}_b$ is the signal used to drive the teleoperated device. The algorithm, described here in the elevation axis only, must, in principle, be implemented in azimuth as well. However, since vibration is primarily along the vertical, the biodynamic interference in azimuth is marginal compared to elevation. For this reason, and practical considerations, the adaptive filter was implemented in elevation only in the experiments described in this paper.

III. Adaptive Filter

The adaptive filter is based on the well-known LMS algorithm widely used in adaptive noise-cancellation applications. It is an extension of the classical LMS described in Widrow and McCool.[10] Its main advantages are small computational load, global stability, and robustness. The extended LMS algorithm presented in this paper has the additional advantages of rapid adaptation to variations in model parameters and the precise estimation of the relatively small disturbance U_b in the presence of large voluntary head motion U_c. This issue is addressed in Merhav.[9] Other algorithms, such as recursive-least-square (RLS) and lattice filters,[11,12] were considered because of their superior convergence in terms of the number of iterations. However, in view of their larger computational complexity, longer iteration times, and lower robustness where rapid variations in model parameters are involved, they were not adopted in the present study. In view of these considerations and the successful implementation of the basic LMS in suppressing biodynamic disturbances in manual control,[13,14] the extended LMS was used in the work described here.

Extended LMS Filter

Figure 2 describes the basic LMS filter in conjunction with the variables and parameters described in Sec. II and in its role of noise suppression. The error e which drives the algorithm is given by

$$e_j = U_{c_j} + U_{b_j} - \hat{U}_{b_j} = U_{c_j} + \tilde{U}_{b_j} \tag{1}$$

where j is the index of the sampled process. The estimation error $\tilde{U}_b$ is given by

$$\tilde{U}_{b_j} = U_{b_j} - \hat{U}_{b_j} \tag{2}$$

where U_c adds to e and upsets the proper convergence of the algorithm. Therefore, in order to assure $\hat{U}_b \to U_b$, it is necessary to fulfill the condition that $U_c \ll U_b$. Assuming that the parameter variations of the human biodynamic model are relatively slow and small, $\hat{U}_b$ converges to U_b with satisfactory precision. The filtered signal U_f therefore is given by

$$U_{f_j} = U_{c_j} + U_{b_j} - \hat{U}_{b_j} = U_{c_j} + \tilde{U}_{b_j} \approx U_{c_j} \tag{3}$$

Equation (3) indicates that the biodynamic interference due to a is essentially canceled. In reality, the condition $U_c \ll U_b$ is not fulfilled. U_c can be in the order of 90 deg or more, while U_b is normally on the order of 1 deg. The variations in the parameters of the human biodynamic model are not necessarily slow. They may be rather rapid as a result of sudden changes in posture or muscle tone. Therefore, the basic filter, as shown in Fig. 2, does not meet all of the requirements. The

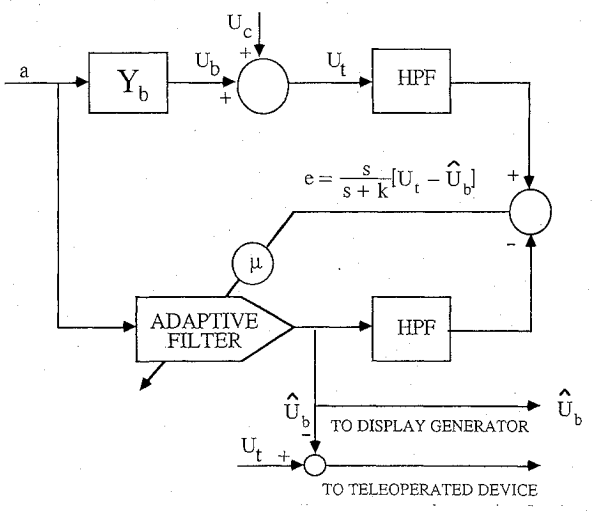

Fig. 3 Extended LMS algorithm for suppression of biodynamic interference in HMD and head teleoperation.

extended LMS filter, which can estimate both U_b and U_c, is shown in Fig. 3. A high-pass filter, for example of the type $s/(s+k)$, is inserted both in the Y_b and the AF path in order to maintain proper phase balance. The error e is now

$$e_j = \frac{s}{s+k}(U_{t_j} - \hat{U}_{b_j}) = \frac{s}{s+k}(U_{c_j} + \tilde{U}_{b_j}) \tag{4}$$

Thus, with the high-pass filters, e is affected by changes in U_c and not by U_c itself. Consequently, the estimated gradient is given by

$$\hat{\nabla}_j = 2e_j \frac{\partial e_j}{\partial w_j} = -2e_j\left\{\frac{s}{s+k}x_j\right\} \tag{5}$$

and the extended LMS algorithm takes the form

$$w_{j+1} = w_j + 2\mu_j e_j\left\{\frac{s}{s+k}x_j\right\} \tag{6}$$

where x_j represents the accelerations a_j, μ_j is the gain, and w is the weight vector. In the actual implementation, a is high-pass filtered in order to reduce the effects of sensor bias and gravity.

The estimate of the nonvoluntary head motion $\hat{U}_b$ is

$$\hat{U}_{b_j} = w_j^T x_j \tag{7}$$

and the estimate of the voluntary head motion U_f is

$$U_{f_j} = U_{t_j} - \hat{U}_{b_j} = U_{c_j} + \tilde{U}_{b_j} \tag{8}$$

In order to assure that the convergence rate of the algorithm is independent of the input intensity x, μ_j is chosen such that

$$\mu_j = \frac{1}{f\,\mathrm{tr}(R_j)} \tag{9}$$

where f is a constant coefficient $f > 1$ and R is the covariance matrix of the input x. This choice of μ_j yields the normalized LMS (NLMS). The spread of the eigenvalues of R is reduced by the square root of the spread as compared to the basic LMS algorithm. The rate of convergence and its sensitivity to eigenvalue spread are substantially reduced.[12]

Rapid adaptation requires a large μ. In accordance with Eq. (9) this implies a small f. The smaller f is, the larger the misadjustment noise in the estimated weight vector w.[10] On the other hand, the smaller μ is, the slower the adaptation rate. A remedy to this conflict is to implement an error dependent $\mu = \mu(\epsilon)$, where $\mu(\epsilon)$ is a monotonic function in e independent of sgn(e). Thus, if e, for example, increases as a result of a change in Y_b, μ is large and the adaptation is rapid. Yet, once convergence proceeds, μ becomes small, and the misadjustment noise becomes small. The implementation of μ is as follows. We choose μ_o in accordance with the stability criterion of the algorithm,[10] namely,

$$\mu_o = \frac{1}{f\,\mathrm{tr}(R_j)} \tag{10}$$

We define

$$e_j \triangleq [e_j,\ e_{j-1},\ \ldots,\ e_j(N'-1)]^T \tag{11}$$

where $N' > N$.

Let

$$e_j^2 \triangleq e_j e_j^T = \sum_{i=j-(N'-1)}^{j} e_i^2 \tag{12}$$

$$\epsilon_j \triangleq \left[\frac{e_j^2}{\mathrm{tr}(R_j)}\right]^{1/2} \tag{13}$$

A possible method to implement $\mu(\epsilon)$ is as follows. We define threshold and saturation values ϵ_t and ϵ_s, and we prescribe

$$\mu_j(\epsilon) = \begin{cases} 0 & 0 \le \epsilon_j < \epsilon_t \\ \dfrac{\epsilon_j - \epsilon_t}{\epsilon_s - \epsilon_t}\mu_{o_j} & \epsilon_t \le \epsilon_j < \epsilon_s \\ \mu_{o_j} & \epsilon_s \le \epsilon_j \end{cases} \tag{14}$$

However, large angular head motion, in spite of the high-pass filter $s/(s+k)$, will still cause large transients in e and perturbations in w. In order to overcome this problem, we set $\mu_j(\epsilon) = 0$ whenever the error e exceeds a given threshold e_o. We divide e into two components, namely, e_c resulting from large head motion, and e_b resulting from the nonvoluntary head motion. Thus,

$$e_j = e_{c_j} + e_{b_j} \tag{15}$$

Whenever $|e_j| > e_o$, $\mu_j(\epsilon) = 0$, and w is frozen; e_o is so chosen that $\mathrm{prob}\{e_j \ge e_o\} \to 1$ whenever the variations in U_c are large. When the variations in U_c are small, the threshold e_o must fulfill the condition $\mathrm{prob}\{e_{bj} \le e_o\} \to 1$. The advantage of freezing the weights is that, after a large change in U_c, only a short time is needed to re-establish a good estimate of U_b. The disadvantage is that during the freezing intervals, parameter tracking is inhibited.

Bias and g components in the accelerometers degrade the convergence of the algorithm and cause errors in the estimate

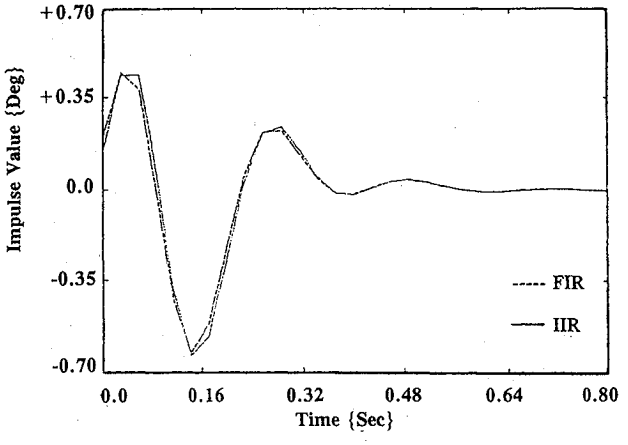

Fig. 4 FIR and IIR for the linear biodynamic model $Y_{b_L}(s)$.

of U_b. This can be overcome by additional high-pass filtering of the accelerometer readings.

Choice of Adaptive Filter Parameters

Three principal parameters are involved: 1) the number of weights N; 2) the length of the delay sequence of the filter T_f in terms of real time as defined in Eq. (16); and 3) the length of the delay interval between samples ΔT. These parameters are related by

$$T_f = (N-1)\Delta T \tag{16}$$

Since normally $N \gg 1$, we have

$$N \cong \frac{T_f}{\Delta T} \tag{17}$$

In order to ensure proper performance of the algorithm, T_f must be longer than the effective length of the infinite impulse response (IIR) of Y_b. This value is usually not known. However, a rough estimate can often be made and T_f can be assigned with some excess margin. The average time constant of convergence of the filter in terms of the number of iterations τ_{it} for the adaptation error to decay to e^{-1} of its original value, in accordance with Widrow et al.,[15] is shown to be determined by

$$\tau_{it} = \frac{fN}{4} \tag{18}$$

In order to ensure a convergence error not greater than 2% of its initial value, the number of iterations τ_{it}, which is required, is $4\tau_{it}$. Therefore, the convergence time constant τ_s is proportional to T_f in accordance with

$$\tau_s = f\left(\frac{T_f}{\Delta T}\right)\Delta T = fT_f \tag{19}$$

The sampling interval ΔT must comply with the sampling theorem, i.e.,

$$\Delta T \leq \pi/\omega \tag{20}$$

where ω is the bandwidth of the input signal $x(t)$.

In addition to the requirement imposed by the sampling theorem, the number of weights N must be sufficiently large so that the finite impulse response (FIR) approximation describes with sufficient fidelity the actual IIR of Y_b. For example, if the IIR contains periodic modes, N must be able to provide at least six samples per period $T = 2\pi/\omega$.

Another factor to be considered is the misadjustment factor M, which is defined as the excess parameter noise in w over the noise in the asymptotic Wiener solution of the LMS.[15] The misadjustment M is given by

$$M = 1/f \tag{21}$$

It is therefore clear that a large value of f reduces M, but increases the number of iterations in accordance with Eq. (18); f is therefore chosen as a compromise between these conflicting factors by trial and error and so are the parameters ϵ_s and ϵ_t in $\mu(\epsilon)$ and the threshold value e_o.

IV. Computer Simulations

In this section, a number of computer simulations of the performance of the adaptive filter with a linear model for Y_b are described. This model was developed with the aid of preliminary experiments. A human subject placed in the moving base simulator was sinusoidally vibrated in the vertical axis at frequencies up to 10 Hz. It was found that in the neighborhood of 5 Hz, Y_b exhibits a resonance with a peak of 12 dB. At frequencies below 1 Hz and above 7 Hz, no significant head motion was observed. These findings are substantiated by previous studies.[16] It follows that $Y_b(s)$ has at least one zero at $s = 0$ and that it sharply cuts off beyond 7 Hz. The

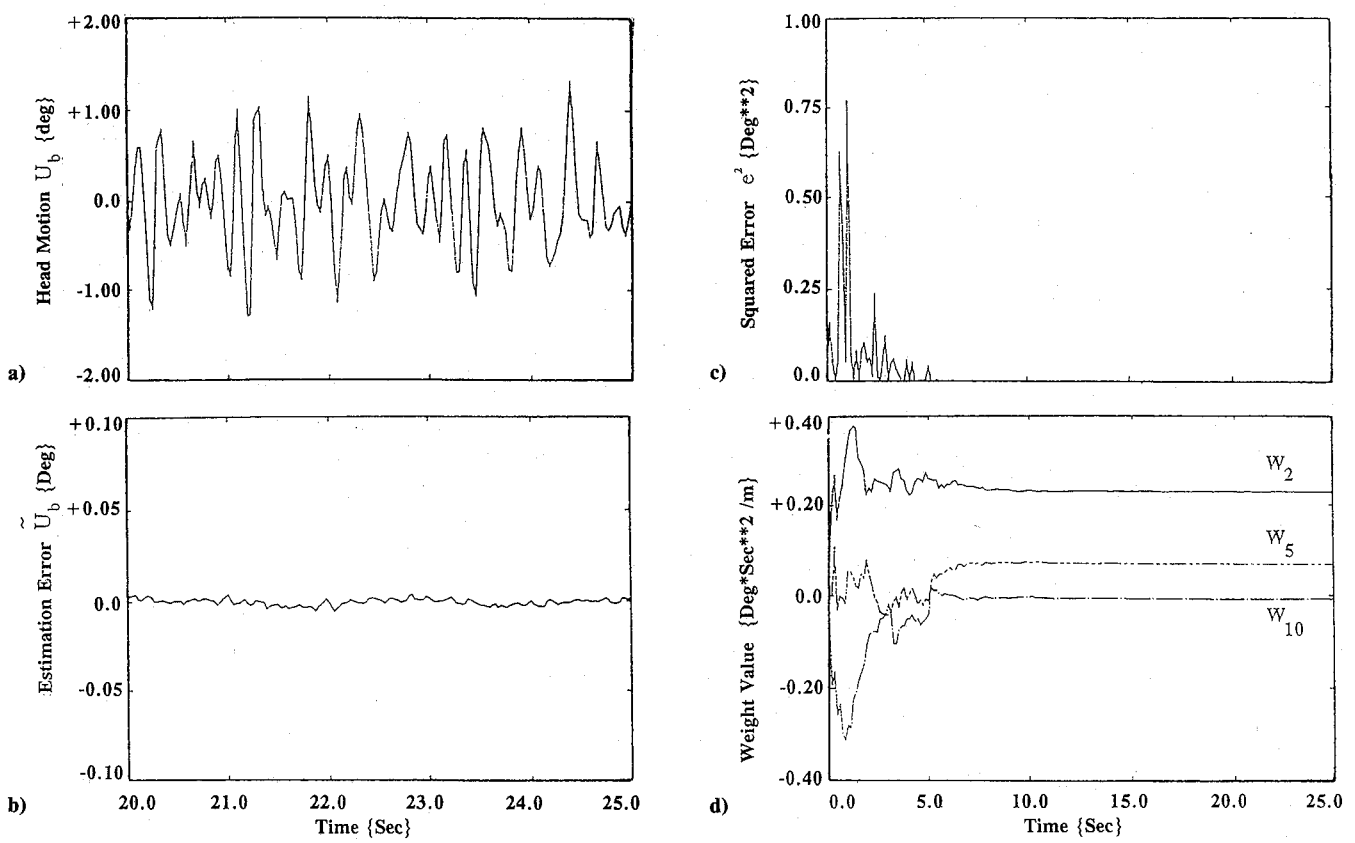

Fig. 5 A section of the time history: a) nonvoluntary head motion; b) estimation error $\tilde{U}_b$; c) square of convergence error e^2; and d) three of the weights, for the example without large head movements.

transfer function that was obtained by a fitting procedure closely describes the experimental results, and is given by

$$Y_b(s) = 3{,}160{,}000 \frac{s^2}{(s+20)^4(s^2+19s+990)}$$

Figure 4 illustrates the impulse response corresponding to $Y_b(s)$.

Adaptive Filter Used in the Simulations

Figure 5 demonstrates that the effective length of the IIR of Y_b is about 0.6 s. The sampling rate in the experimental setup is 37 ms. This rate was also chosen for the computer simulations. N was set to 30 in order to provide acceptable fidelity and to avoid FIR truncation due to insufficient length T_f which was set to 0.81 s. The high-pass filter $s/(s+k)$ was set to have a break point at 1 Hz. The other filter parameters were chosen in accordance with the guidelines in Sec. III and by a cut-and-try approach. Thus, the following values were chosen: $f = 2$; $\epsilon_s = 0.001$; $\epsilon_t = 0.0011$; and $\epsilon_0 = 0.5$. The initial conditions were $w = 0$ and $x = 0$.

Suppression of Interference with Small Head Motion

The purpose of this simulation is to test the performance of the algorithm in the simple case of small voluntary head motion U_c. The simulated vertical acceleration that excited the model, $Y_b(s)$, was obtained by passing Gaussian white noise through a second-order low-pass filter with a cutoff frequency of 30 Hz and a damping factor of 0.5. The nonvoluntary head motion U_b, which resulted from this excitation, is described in Fig. 5a. Figure 5b shows that the estimation error $\tilde{U}_b$ is less than 1% of U_b. This result demonstrates the high estimation precision that can be obtained. In this example, since $U_c = 0$, $U_f = \tilde{U}_b$. The square of the convergence error e^2 is shown in Fig. 5c. The convergence history of three of the weights is shown in Fig. 5d. These two figures indicate that the convergence time is about 7 s, which permits on-line operation. Figure 5d also demonstrates the small misadjustment noise achieved by the algorithm. Figure 4, which compares the estimated FIR of Y_b, which consists of the values to which the 30 weights of the algorithm have converged, with the IIR describing $Y_b(s)$, demonstrates their excellent correspondence.

Suppression of Interference with Large Head Motion

In this example, the acceleration a and U_b are the same as in the foregoing example. Now, U_c adds to U_b and it is shown in Fig. 6a along with U_t. Figure 6b shows U_c along with its estimate U_f. Figure 6c demonstrates that during large variations in U_c, $\tilde{U}_b$ is about 0.75 deg peak-to-peak. It constitutes about 3.75% of estimation error of U_c, and about 37% of U_b. Figure 6d demonstrates the rapid reconvergence of the weights after the transient of the large head motion U_c is over, and their freezing during the transient provided by the freezing logic described in Sec. III.

Effects of Parameter Jumps, Accelerometer Offsets, and Vibration Bandwidth

The purpose of this simulation is to investigate the performance of the adaptive filter in the presence of sudden model parameter jumps. In this example, the gain of the model $Y_b(s)$ was increased by 50%, at 15 s after the beginning of the simulation run that was started as described in the foregoing example. Figure 7 demonstrates the jumps in the weights and their reconvergence to their new values within about 4 s. The comparison of FIR with the IIR of the model after the 50% gain jump demonstrates an excellent fit.

Offsets in the accelerometer cause an increase in convergence time of the algorithm, and they may even prevent proper operation of the filter. The increase in convergence time is a

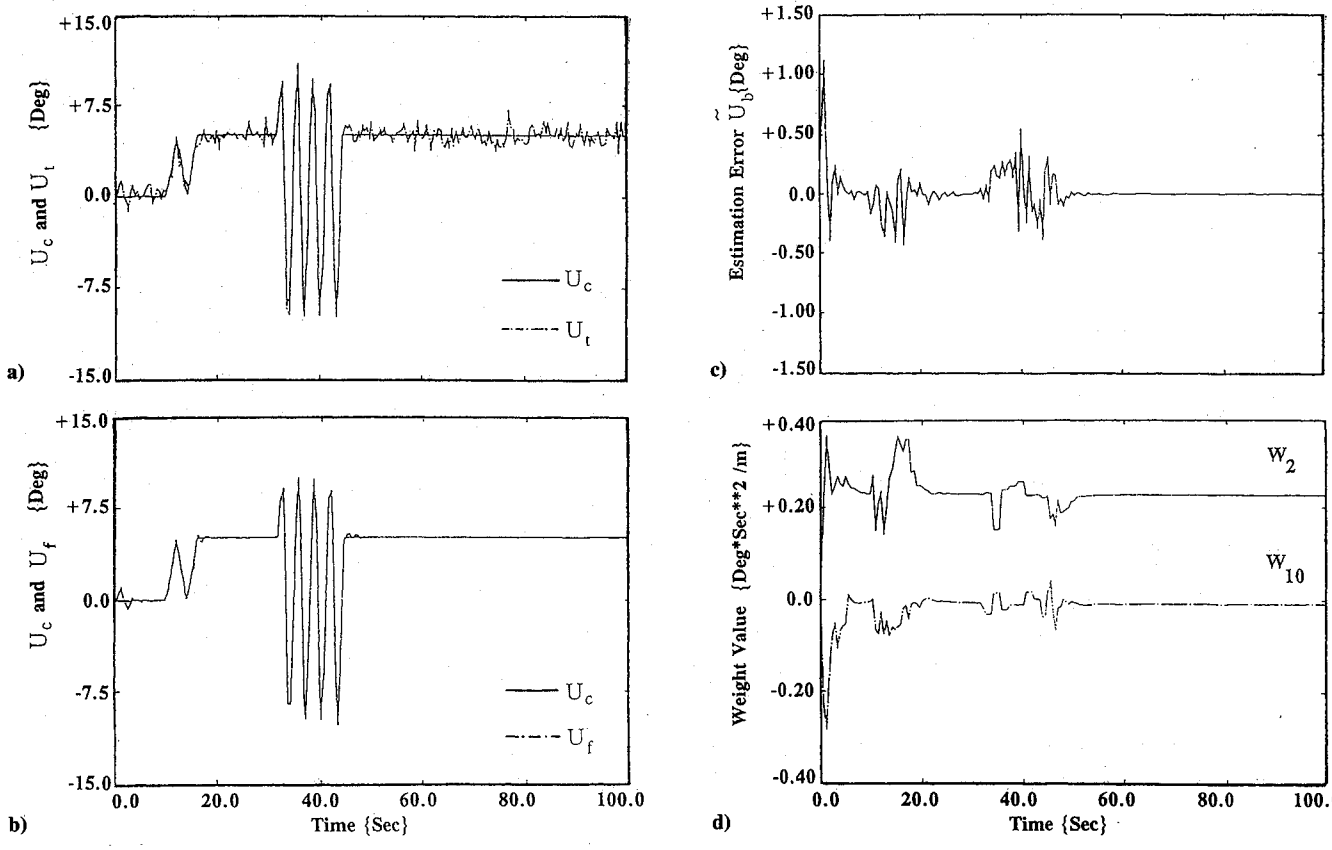

Fig. 6 Time history: a) total and voluntary head motion; b) voluntary motion and its estimation; c) estimation error $\tilde{U}_b$; and d) two of the weights, for the example with large head motion.

result of the settling time of the high-pass filter $s/(s+k)$. An additional high-pass filter, located in both AF and $Y_b(s)$ paths with a break frequency in the order of magnitude of 0.5 Hz, ensures proper convergence of the algorithm but with a slight increase of 15% in $\tilde{U}_b$.

To achieve proper convergence of the weights w in the LMS filter, it is necessary to assure a sufficiently wide band excitation signal of Y_b. In the real environment of the aircraft, this condition is normally not met. With narrow-band excitation, the adaptation error e^2 still converges to zero, but w will normally not converge to the correct values. This, however, does not prevent precise estimation of U_b and U_f which only requires the vanishing of e^2.

The modeling, filter design, and computer simulation described in this section indicate that the methodology of adaptive noise cancellation has the potential to adapt to rapid parameter variations, and to identify U_b in the presence of large values of U_c. This, however, must be validated by actual man-in-the-loop experiments that are described in the next section.

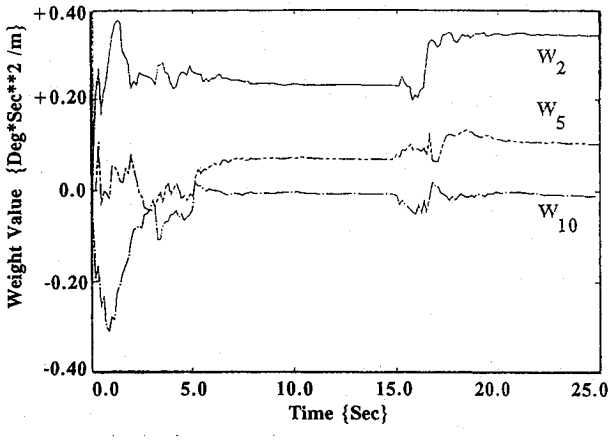

Fig. 7 A section of the time history of three of the weights for the example with parameter jumps.

V. Experimental Validation

The purpose of the experimental validation described in this section is to examine the validity of the assumed model $Y_b(s)$ and to study the performance of the adaptive filter with real human subjects and in the real physical environment of a vibrating platform driven by signals similar to actual helicopter vibration spectra, and which includes unknown nonlinearities, such as in the seat, or additional noise and imperfections in the accelerometers, head motion sensor and display systems. In the experiments, it was not yet possible to directly validate the suppression of display blurring for the following reasons:

1) The lack of a helmet-mounted display with the necessary resolution that permits the display of sufficiently small characters and symbols for which blurring becomes significant.

2) Limitations in the sampling rate of the head motion sensor and the display system which amounted to 40 ms and caused phase shifts in the order of 70 deg at typical vibration frequencies in the region of 5 Hz. Such phase shifts prevent effective image stabilization as outlined in Sec. II.

In spite of these present shortcomings, it was possible to put together a simulation setup for man-in-the-loop experiments. This setup incorporates the following subsystems: 1) six-degree-of-freedom simulator; 2) cabin-mounted accelerometer; 3) system for measuring head motion in six degrees of freedom; 4) light Air-Force-type helmet equipped with the head motion sensor; 5) Digital VAX 750 computer; 6) Motorola VME system 1131 computer; 7) TV Barco display generation and projection system; and 8) interfaces for sampling and communication between subsystems.

This setup can also emulate the function of a helmet-mounted display or sight in its roles in head target tracking and pointing which also underlie the functions of head teleoperation.

Viewing Experiments

Subjects, seated in the simulator cabin one at a time, were instructed to carry out the following tests:

1) View freely a fixed point on the cabin panel to ensure small head motion.

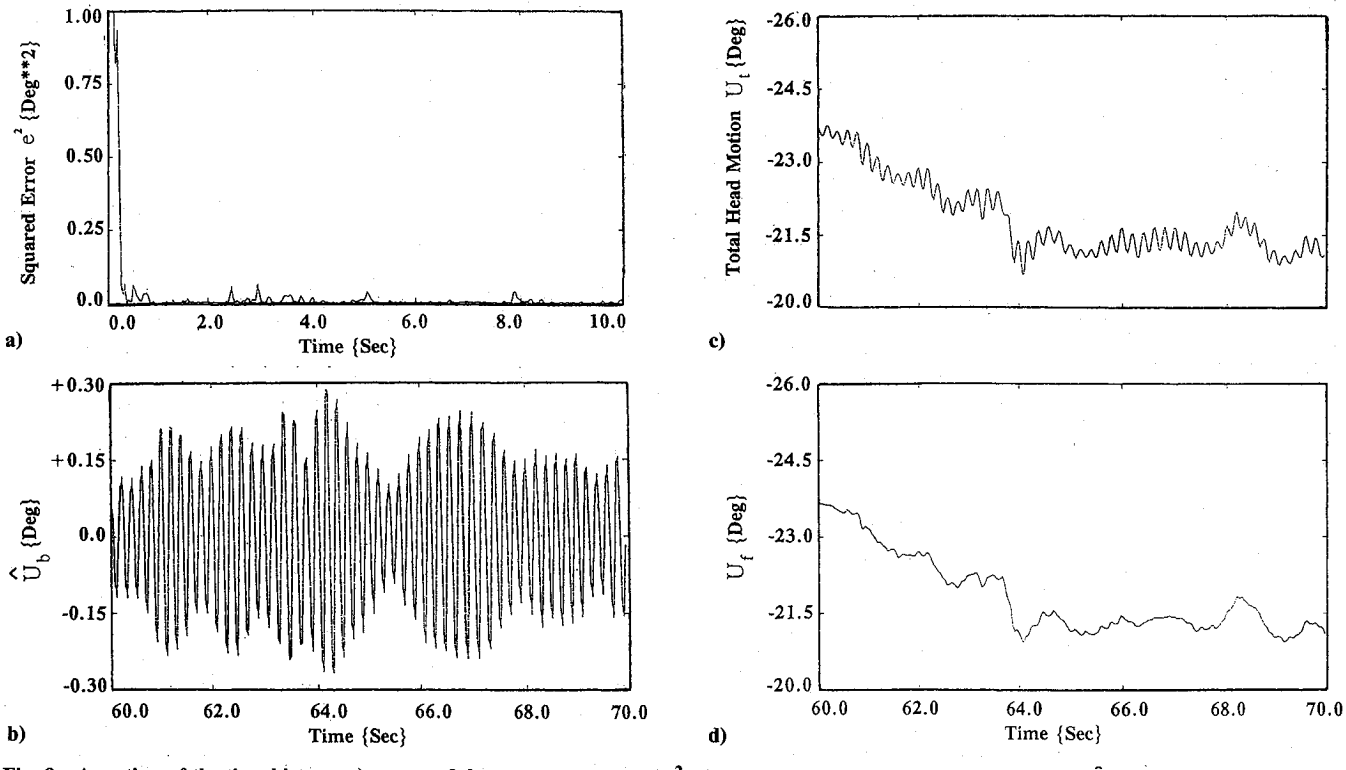

Fig. 8 A section of the time history: a) square of the convergence error e^2; b) estimated nonvoluntary head movement $\hat{U}_b$; c) total head movement U_f; and d) estimated voluntary head movement U_f, for the example with single sine excitation and without large head movement.

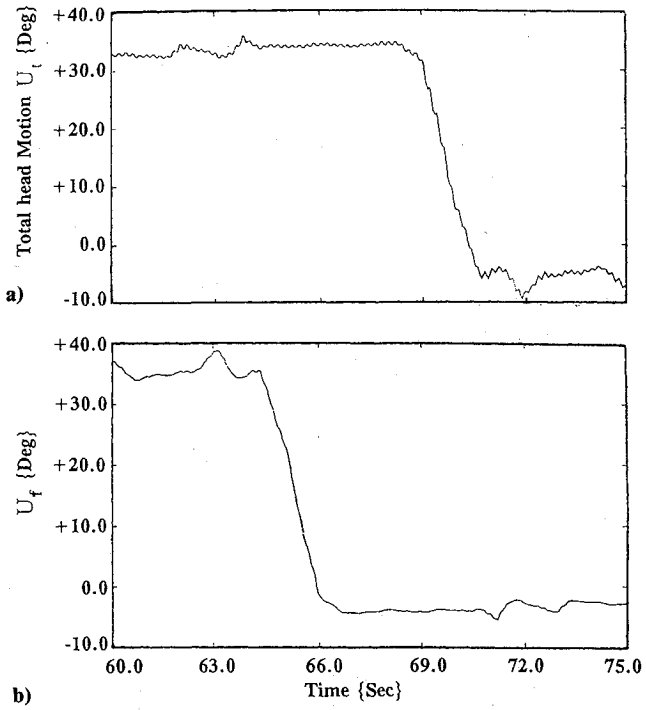

Fig. 9 A section of the time history: a) total head movement U_t; and b) estimated voluntary head movement U_f, for the example with single sine excitation and large head movement.

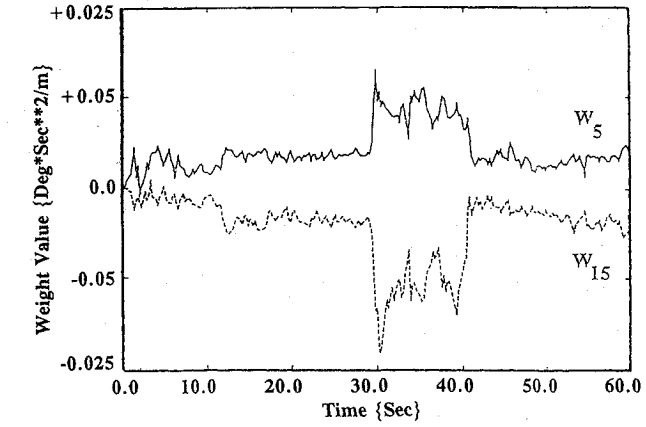

Fig. 10 A section of the time history of two of the weights, for the example with single sine excitation and with changes in biodynamic parameters.

2) Execute large head motion in elevation starting and returning to the fixed point.

3) While viewing the fixed point, change posture and tighten and relax muscles to cause variations in Y_b.

The cabin was vibrated at accelerations up to 0.33 g and up to frequencies of 10 Hz. The vibration consisted of sums of sines and/or of a Gaussian white process filtered by a second-order low-pass filter with various cutoff frequencies. Each run lasted 90 s. The first 15 s were assigned for the convergence of the adaptive filter and for proper settling in the seat. During the remaining 60 s the test was carried out. Data were recorded for the last 75 s. The recorded data were cabin accelerations and head motion. The signals served as the inputs to the adaptive filter that was operating in real time, and its parameters and outputs were also recorded. Ten subjects participated in these tests.

Adaptive Filter

The parameters of the adaptive filter were chosen in accordance with the computer simulations described in Sec. IV. The length of the filter T_f, in accordance with Y_b described in Sec. IV, was set to 0.81 s. The sampling frequency was 37 Hz so that $\Delta T = 27$ ms, and the number of weights was set to $N = 30$. The threshold value was set to $e_o = 1$, and the break frequency of the high-pass filter for U_t was set to 2.4 Hz.

Results of Viewing Experiments

Three examples, demonstrating the performance of the adaptive filter, are given for the three different tests. The vibration conditions for the examples shown for tests 1 and 2 were sinusoidal vertical vibrations at 5 Hz with an amplitude of 0.156 g rms, and in the example given for the third test the subjects were vibrated sinusoidally at 5 Hz and 0.069 g rms. During all of the tests the subjects viewed a fixed point on the panel.

Interference Suppression Without Large Head Motion

Figure 8a demonstrates the rapid convergence of e^2 in the adaptive filter, which permits good estimates of U_b and U_c. Figure 8b describes $\hat{U}_b$, which is about 0.5 deg peak-to-peak and, as anticipated, is at 5 Hz. It is accompanied by low-frequency interferences that are due to small uncontrollable head motion. Figure 8c shows $U_t = U_c + U_b$. The 5-Hz component U_b is clearly visible along with the small variation of U_c. Figure 8d, demonstrating U_f, shows that U_b has almost been entirely removed without affecting U_c. The gradual drift downward is due to a slow unintentional head motion which cannot be prevented in the simple viewing experiment described here and which does not incorporate a reticle that could have prevented this drift. For vibration tests with two or more sines and/or a random component, not shown here, the performance of the filter was comparable with the results shown in Fig. 8. In all examples of vibration, the adaptive filter is effective in identifying U_b even though the excitation of the human body is not rich and Y_b is not well represented by the corresponding FIR. The decisive factor in identifying U_b is the good convergence of e^2.

Interference Suppression with Large Head Motion

Figure 9 shows the performance of the extended LMS adaptive filter in the presence of large head motion. The vibration was at 5 Hz and 0.23 g rms. Figure 9a shows a 15-s section of large head motion U_c accompanied by the small 5-Hz vibration. Figure 9b shows U_t, demonstrating that U_b has almost entirely been removed.

Interference Suppression with Parameter Variations in Y_b

Subjects were vibrated at 5 Hz and 0.069 g rms. At the instant $t = 30$ s, the subject suddenly changed his posture from erect leaning to forward crouching without contact of his back with the chair support while tightening his torso and limb muscles as hard as he could. After 10 s, the subject returned to his original posture. Again, the subject was instructed to view the fixed point on the panel. The history of e^2 demonstrates the sensitivity of the filter to the parameter variations, its rapid adaptation to this change, and the rapid re-adaptation at 40 s as expected. Figure 10 shows the corresponding variations of w_5 and w_{15}. It also shows that after about 2 s, the weights reconverge to almost their original values. The results also demonstrate that during the crouching posture the parameter noise is larger than during the erect posture, probably because it is more difficult to maintain constant levels in muscle tone in the crouching position with tightened muscles.

Comparison of the weights' time histories in Fig. 10 with those of the analytical model in Fig. 7 shows that, in reality, the weights vary all of the time, clearly, because of the persistent variations in posture and muscle tone.

VI. Conclusions

The results shown in this paper demonstrate that the extended least-mean-square filter estimates U_c and U_b rapidly

and accurately. In view of the very small value of $\tilde{U}_b/U_b$, the application of the algorithm to actual helmet-display systems strongly indicates that display blurring due to vibration can be eliminated with the proposed filter algorithm. Very good performance has also been demonstrated in the presence of very large and sudden head motion and changes of posture and muscle tone. The analytical model proved very useful in the choice of the design parameters of the adaptive filter. The results also demonstrate that the image stabilization method based on adaptive filtering does not entail lengthy transients after a large head motion or parameter variation. A general conclusion is that the methodology of least-mean-square filtering is sufficiently robust to withstand the discrepancies between the actual dynamics involved and the linear model used in the computer simulations. Clearly, the results demonstrate that the algorithm is directly applicable to the improvement of precision in tracking and pointing in head teleoperated devices. Very good agreement was found between the real system, involving human subjects and numerous nonlinearities, and the linear model assumed in the concept development.

Acknowledgments

This work has been supported in part by the Human Factors Division, NASA Ames Center, and by the USAF Aerospace Medical Research Laboratory, Wright-Patterson AFB, under Grants NAWG 1128 and AFOSR88 0298, respectively. This paper is based on the M.Sc. thesis of the first author.

References

[1]Levison, W. H., Baron, S., and Junker, A. M., "Modeling the Effects of Environmental Factors on Human Control and Information Processing," Wright-Patterson AFB, OH, AMRL-76-74, Aug. 1976.

[2]Jex, H. R., "Problems in Modeling Man-Machine Control Behavior in Biodynamic Environments," *Proceedings of the 7th Annual Conference on Manual Control,* NASA SP-281, Scientific and Technical Information Office, NASA, Washington, DC, 1971, pp. 3–13.

[3]Wells, M. J., and Griffin, M. T., "A Review and Investigation of Aiming and Tracking Performance with Head Mounted in Sights," *IEEE Transactions on Systems, Man and Cybernetics,* Vol. SMC-17, No. 2, 1987, p. 210–221.

[4]Wells, M. J., and Griffin, M. J., "Tracking with the Head During Whole-Body Vibration," *Training, Human Decision Making, and Control,* edited by J. Patrick and K. D. Duncan, Elsevier, New York, 1988.

[5]Lewis, C. H., and Griffin, M. J., "Predicting the Effects of Vertical Vibration, Frequency, Combination of Frequencies, and Viewing Distance on the Reading of Numeric Displays," *Journal of Sound and Vibration,* Vol. 70, No. 3, 1980, pp. 355–377.

[6]Wells, M. J., and Griffin, M. J., "Benefits of Helmet-Mounted Display Image Stabilization Under Whole-Body Vibration," *Aviation, Space, and Environmental Medicine,* Vol. 55, No. 1, 1984, pp. 13–18.

[7]Benson, A. J., and Barnes, G. R., "Vision During Angular Oscillation: The Dynamic Interaction of Visual and Vestibular Mechanisms," *Aviation, Space, and Environmental Medicine,* Vol. 49, No. 4, 1978, pp. 557–564.

[8]Wells, J. M., and Griffin, M. J., "Flight Trial of a HMD Image Stabilization System," *Aviation, Space, and Environmental Medicine,* Vol. 58, No. 4, 1987, pp. 319–323.

[9]Merhav, S. J., "Adaptive Suppression of Biodynamic Interference in Helmet-Mounted and Head-Down Displays," AIAA Paper 88-4185, Aug. 1988.

[10]Widrow, B., and McCool, J. M., "A Comparison of Adaptive Algorithms Based on the Method of Steepest Descent and Random Search," *IEEE Transactions on Antennas and Propagation,* Vol. AP-24, No. 5, 1976, pp. 615–637.

[11]Haykin, S., *Adaptive Filtering Theory,* Prentice-Hall Information Systems Science Series, Prentice-Hall, Englewood Cliffs, NJ, 1986.

[12]Honig, M. L., and Messerschmitt, D. G., *Adaptive Filters, Structures, Algorithms, and Applications,* Kluwer Academic Publishers, Norwell, MA, 1984.

[13]Velger, M., Grunwald, A., and Merhav, S., "Suppression of Biodynamic Disturbances and Pilot-Induced Oscillations by Adaptive Filtering," *Journal of Guidance, Control, and Dynamics,* Vol. 7, No. 4, 1984, pp. 401–409.

[14]Velger, M., Grunwald, A., and Merhav, S., "Adaptive Filtering of Biodynamic Stick Feedthrough in Manipulation Tasks on Board Moving Platforms," *Journal of Guidance, Control, and Dynamics,* Vol. 11, No. 2, 1988, pp. 153–158.

[15]Widrow, B., McCool, J. M., Larimore, M. G., and Johnson, C. P., "Stationary and Nonstationary Learning Characteristics of the LMS Adaptive Filter," *Proceedings of the IEEE,* Vol. 64, No. 8, Aug. 1976.

[16]Griffin, M. J., "The Transmission of Triaxial Vibration to Pilots in the Scout AH MK1 Helicopter," Univ. of Southampton, Inst. of Sound and Vibration, TR 58, Southampton, England, UK, Aug. 1972.